Classification of Carbide Distributions using Scale Selection and Directional Distributions

Klaus Wiltschi[1], Tony Lindeberg[2], Axel Pinz[1]
[1]Institute for Computer Graphics and Vision, TU-Graz, A-8010, Austria
[2]Computational Vision and Active Perception Laboratory, KTH, S-100 44, Stockholm, Sweden

Abstract

We present an automatic method for the classification of steel quality based on scale-space operations. The carbide distribution of microscopic specimen images is assessed by classifying according to so-called 'degree' and 'type' of the specimen. 'Degree' is represented by features extracted with automatic scale selection, and 'type' information is computed from second-moment descriptors. In combination with a morphological verification scheme, this pattern classifier shares large similarities with current manual techniques. Compared to previous work, the new classification scheme has several advantages: The significant scale of the carbide agglomeration is calculated explicitly, and the method is less sensitive to the variance of spatial connectivity than a morphological approach.

1 Introduction

In the production of high speed steel, the rolling affects the micro-structure of the steel, which in turn influences the mechanical properties. Specifically, the distribution of carbide is essential, since cracks propagate within the carbide agglomerations [14]. Thus, the classification of carbide distributions is an important task in quality control. Currently, specially skilled metallographers classify the carbide distributions using a light microscope at a magnification of 1:100 by assigning them to a standard chart of 28 images, arranged in 4 rows and 7 columns as shown in Fig. 1. Carbide distributions are distinguished according to visually captured features, referred to as the *'degree'* and the *'type'* of the carbide agglomerations (i.e. the white dense areas of carbide particles). In each row (degree), the size of the agglomerations increases from left to right, whereas in each column (type), the shape ranges from band-shaped to net-shaped structures from top to bottom, caused by the stretching of originally net-shaped structures during the rolling process. The standard chart can be interpreted as categorizing the carbide distributions into 4×7 classes according to *type* and *degree*.

The subject of this article is to present a method which performs this classification automatically based on recently developed computer vision tools for feature detection with automatic scale selection [10, 9, 11] combined with texture descriptors derived from second moment descriptors [1, 10, 4, 12]. The image descriptors obtained in this way are then verified by a morphological scheme [13, 14].

2 Scale selection module

To handle the inherent multi-scale nature of image data, the notion of scale-space theory has been developed [15, 6, 8, 3, 10]. For any N-dimensional image $f: \mathbb{R}^N \to \mathbb{R}$, its *scale-space representation* $L : \mathbb{R}^N \times \mathbb{R}_+ \to \mathbb{R}$ is defined by

$$L(\cdot;t) = g(\cdot;t) * f(\cdot) \tag{1}$$

where $g : \mathbb{R}^N \times \mathbb{R}_+ \to \mathbb{R}$ denotes the N-dimensional Gaussian kernel:

$$g(\cdot;t) = \frac{1}{(2\pi t)^{N/2}} e^{\frac{-(x_1^2+\cdots+x_N^2)}{2t}} \tag{2}$$

and the variance $t \in R^+$ of the Gaussian kernel is referred to as the *scale parameter*. Based on this representation, *scale space derivatives* are defined by

$$L_{x^\alpha}(\cdot;t) = \partial_{x_1^{\alpha_1} \ldots x_N^{\alpha_N}} L(\cdot;t) = (\partial_{x_1^{\alpha_1} \ldots x_N^{\alpha_N}} g(\cdot;t)) * f(\cdot) \tag{3}$$

with corresponding *normalized derivatives* given by

$$\partial_{\xi_i^n} = t^{n/2} \partial_{x_i^n}. \tag{4}$$

Many feature detectors can be formulated as (linear and non-linear) combinations of partial derivatives. Specifically, scale levels for feature detection can be selected by detecting local extrema over scales of such differential geometric descriptors [9, 10, 11].

2.1 Feature detection and ranking

Since the agglomerations mainly form blob- or ridge-like structures, a *ridge detector*, which builds upon the earlier methods for ridge detection described

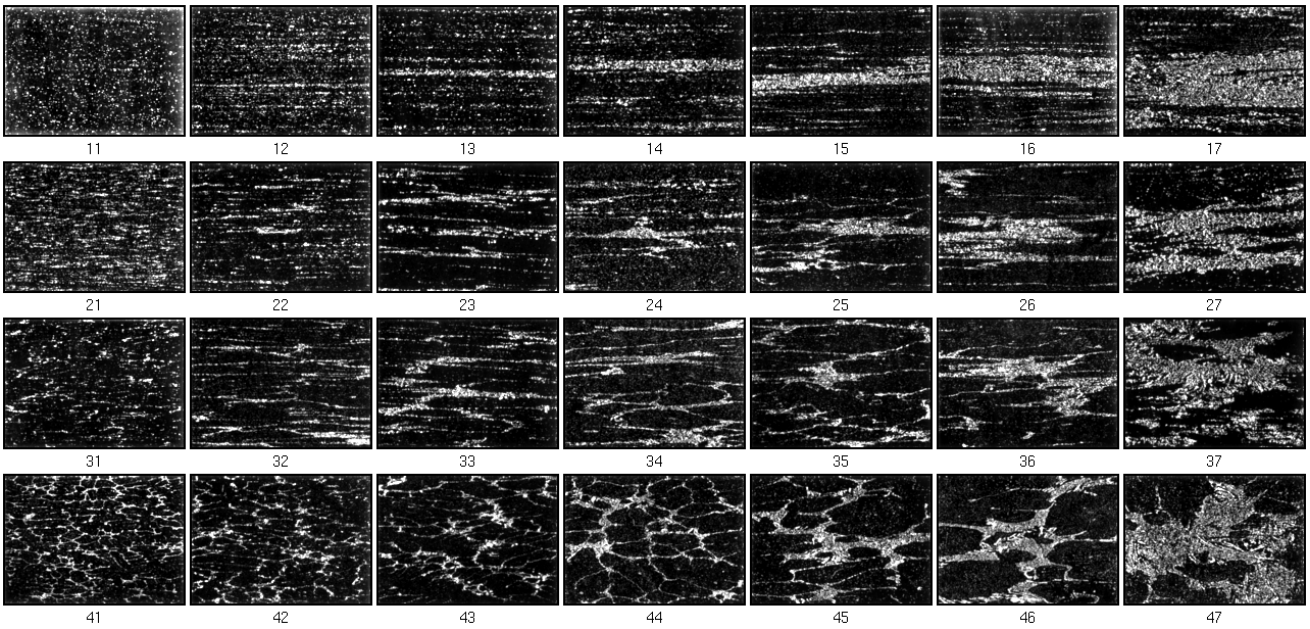

Figure 1: The microscopic standard chart for characterizing carbide distributions of high speed steels (white dots represent carbide particles). The row index (1..4) denotes the *type* of the distribution, which corresponds to the *shape* of the agglomerations. The column index (1..7) describes the *degree*, basically reflecting the *size* of the agglomerations.

in [5, 2, 7] is defined as follows [11]: Introduce a local (p, q)-coordinate system at each image point, defined by the mixed second-order derivative being zero (*i.e.*, $L_{pq} = 0$). Then, we can detect (possibly elongated, bright) blob features from points which are simultaneously maximal with respect to space and scales in

$$-L_{pp,norm} = -t\, L_{pp} \tag{5}$$

where L_{pp} is the principal curvature having the largest absolute value. To rank these features on significance, we weigh the normalized response $L_{pp,norm}$ at each scale-space maximum by $\sqrt{t}$, which gives the *significance measure*

$$S(A) = -\sqrt{t}\, L_{pp,norm}(x, y). \tag{6}$$

An intuitive motivation for this weighting is that the width of the ridge feature can be expected to be proportional to $\sqrt{t}$. Figure 2(a) shows the result of applying this operation to image 33 of the reference chart.

Certain image structures give rise to multiple responses. To suppress overlaps, a scale-space maximum A is rejected if there exists another maximum B and

$$\begin{aligned} &\text{center}(A) \in \text{support region}(B) \ \wedge \\ &\text{center}(B) \in \text{support region}(A) \ \wedge \\ &t_A/t_B \in \left[\tfrac{1}{\alpha}, \alpha\right] ; \ (\alpha > 1) \ \wedge \ S(A) < S(B) \end{aligned} \tag{7}$$

with $\alpha = 4$ corresponding to a ratio of 2 between the blob radii (see Fig. 2(b)).

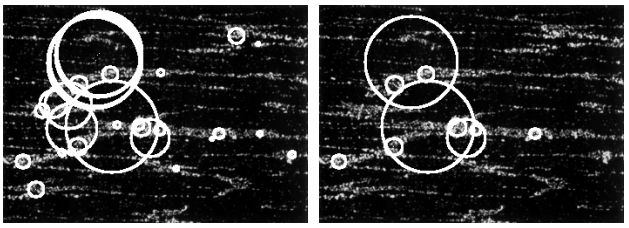

(a) 30 most significant resp. (b) overlap suppression (10)

Figure 2: The most significant ridge features detected from equations (5) and (6). Each response is illustrated by a circle with the radius proportional to the selected scale.

2.2 Feature verification

To suppress spurious responses from the feature detection module ('false alarms'), we use the following verification mechanism, which constitutes an extension of a previously developed morphological module for perceptual grouping of substructures [13, 14]:

1. An elliptical support region is associated with each detected scale-space maximum based on the two principal curvatures $L_{pp,norm}/L_{qq,norm}$ as well as the orientation of the ridge. Starting from an idealized two-dimensional elliptical blob model defined by

$$g(x, y; t) = \frac{1}{\sqrt{2\pi t_1}} e^{\frac{-x^2}{2t_1}} \frac{1}{\sqrt{2\pi t_2}} e^{\frac{-y^2}{2t_2}}, \tag{8}$$

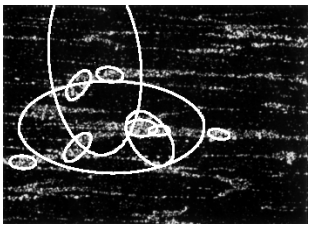

(a) Elliptical support regions.

(b) Characteristic structure.

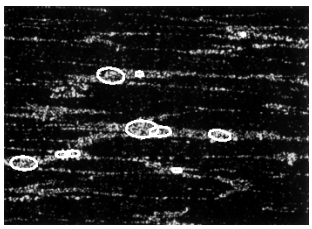

(c) Verified structures.

Figure 3: Verification of the most significant entities using a *characteristic structure*.

the ratio t_2/t_1 between the major and the minor axis of the ellipse can be estimated as

$$\frac{t_2}{t_1} = \frac{1}{2}\left(3\,\frac{L_{pp,norm}}{L_{qq,norm}} - 1\right); \qquad t_1 := t, \tag{9}$$

where an upper bound of $t_2/t_1 \leq 2$ is used to prevent overestimation [11]. Within each such support region the following verification scheme is applied:

2. A binary mask of the *characteristic structure* in the image is generated by adaptive thresholding followed by morphological opening and closing yielding a binary image showing connected components for the carbide agglomerations (see Figure 3(b) and [13]).

3. The largest non-overlapping circular opposite regions in the support region are computed by detecting local extrema in an Euclidean distance map.

4. The areas of these opposite regions are used for suppressing responses with interfering substructures.

5. The k most significant extrema are selected, and the radius R_{detect} of the largest extremum is used as a size description feature for the classification of the carbide distribution according to the *degree*, i.e.

$$R_{detect} = \sqrt{2\,t_{detect}\,\log 2}; \qquad t_{detect} = \max(t_1, \ldots, t_k) \tag{10}$$

where $k = 10$. This size descriptor is illustrated in Figure 4, where the largest detected structures are marked (the length of the minor axes of the ellipse is equal to R_{detect}) for 2 neighboring reference images.

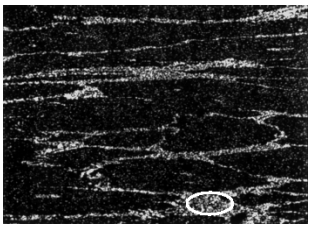

(a) Reference image 34

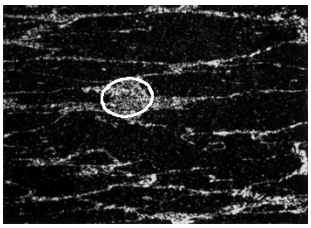

(b) Reference image 35

Figure 4: The largest structures obtained by applying the composed detection/verification procedure to two neighboring columns in the reference chart.

3 Shape estimation

3.1 The multi-scale windowed second moment matrix

To represent directional distributions, the second moment matrix is a useful texture descriptor [1, 4, 12]. Given a symmetric normalized window function w, the *windowed second moment matrix* can be defined by

$$\mu_L(\mathrm{q}) = \int_{\mathrm{x}\in\mathbb{R}^2} (\nabla L(\mathrm{x}))(\nabla L(\mathrm{x}))^T w(\mathrm{q}-\mathrm{x})d\mathrm{x}, \tag{11}$$

where $L : \mathbb{R}^2 \to \mathbb{R}$ denotes the image brightness and $\nabla L = (L_x, L_y)^T$ its gradient. Denoting the windowing operation by E_q, Equation (11) can be written as

$$\begin{aligned} \mu_L(q) &= \begin{pmatrix} \mu_{11} & \mu_{12} \\ \mu_{21} & \mu_{22} \end{pmatrix} = E_q \begin{pmatrix} L_x^2 & L_xL_y \\ L_xL_y & L_y^2 \end{pmatrix} \\ &= E_q((\nabla L)(\nabla L)^T) \end{aligned} \tag{12}$$

and from the components of μ_L, the following descriptors can be defined

$$P = E_q(L_x^2+L_y^2), \quad C = E_q(L_x^2-L_y^2), \quad S = 2E_q(L_xL_y). \tag{13}$$

P is a measure for the strength of the operator response, C and S contain directional information, which can be summarized in two anisotropy measures

$$Q = \sqrt{C^2+S^2}, \qquad \tilde{Q} = Q/P. \tag{14}$$

The *normalized anisotropy* $\tilde{Q} \in [0;1]$ is zero, if and only if $E_q(L_x^2) = E_q(L_y^2)$ and $E_q(L_xL_y) = 0$ and $\tilde{Q} = 1$ if and only if $E_q(L_xL_y) = E_q(L_x^2)E_q(L_y^2)$. A rotationally symmetric gray-level pattern has $\tilde{Q} = 0$ and a translationally symmetric pattern has $\tilde{Q} = 1$.

When computing this descriptor in practice, the gradient vectors are defined at *local scale* t_l and we use a Gaussian window function g with *integration scale* t_i [10, chap. 14]. Therefore, the *multi-scale windowed second moment matrix* μ_L is defined as

$$\mu_L(\mathrm{q};t_l,t_i) = \int_{\mathrm{x}\in\mathbb{R}^2} (\nabla L(\mathrm{x}))(\nabla L(\mathrm{x}))^T g(\mathrm{q}-\mathrm{x};t_i)d\mathrm{x}. \tag{15}$$

3.2 Scale selection to compute anisotropy

The directional distribution (*type*) of the carbide distribution can be modeled by evaluating the $\mu_L(\mathrm{q}; t_l, t_i)$ based on the scale information of the scale selection scheme described in section 2. Therefore, the normalized anisotropy $\tilde{Q}$ is calculated for

$$t_l = \gamma_l * t_{detect}, \tag{16}$$

where $\gamma_l = 0.5$, which is chosen to maximize the classification performance of the resulting shape description feature $\tilde{Q}$ according to the *type* (see section 4).

Assuming a globally valid significant scale for each image, the integration scale is set to the size of the image. Global values of P, C and S are computed by summing up the corresponding gradient expressions over the whole image and determining global values of Q and $\tilde{Q}$ afterwards. This yields a shape description feature for classifying carbide distributions according to their *type* (see section 4):

$$\tilde{Q}_{detect} = \tilde{Q}(\mu_L(x, y; t_l, \text{image size})) \tag{17}$$

4 Classification results

To evaluate the size and shape descriptors obtained from the composed feature detection scheme, we used a reference data base consisting of 429 images, which was then split up into a training set of 290 carbide distributions and a disjunct test set with 139 images. The performance of the features extracted from the data was evaluated by a minimum distance classifier.

To assess the performance of R_{detect} governing the determination of the *degree* (size) of the carbide distribution, all images of the same *degree* were combined into one class, yielding 7 degree classes. In a similar manner, we produced 4 type classes to evaluate the performance of $\tilde{Q}_{detect}$ determining the *type* (shape) of the carbide distribution.

The classification rates of the resulting minimum distance classifiers for *degree* and *type* are shown in table 1. We give the percentages of images classified to the correct or to a directly neighboring class, allowing a one step class deviation, which is also quite common in the visual classification by the metallographers.

	correct [%]	one class deviation [%]
R_{detect} (*degree*)	50	93
$\tilde{Q}_{detect}$ (*type*)	45	80

Table 1: Minimum distance classification performance.

Figure 5 shows mean and standard deviation of the features for the whole sample set of 429 images. There is a large variance in the values of $\tilde{Q}_{detect}$ for type 1 because no anisotropic (band-like) structures occur in the very fine-scale carbide structures (cf. fig. 1), resulting in a low anisotropy value, similar to net-shaped structures. This drawback of low discrimination for the lowest degrees can be eliminated by including selected features from previous work [13].

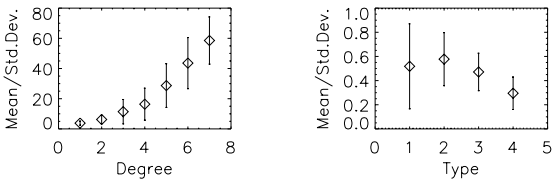

(a) *degree* feature R_{detect} (b) *type* feature $\tilde{Q}_{detect}$

Figure 5: Mean and StdDev for *degree* and *type*.

References

[1] Bigün et al. *Multidimensional orientation estimation with applications to texture analysis and optical flow,* PAMI, 13(8):775–790, 1991.

[2] Eberly et al. *Ridges for image analysis,* Mathematical Imaging and Vision 4(4):353–373, 1994.

[3] Florack et al. *Scale and the differential structure of images,* IVC 10(6):376–388, 1992.

[4] Gårding, Lindeberg. *Direct computation of shape cues using scale-adapted spatial derivative operators,* IJCV 17(2):163–191, 1996.

[5] Haralick. *Ridges and valleys in digital images,* CVGIP 22:28–38, 1983.

[6] Koenderink. *The structure of images,* Biol.Cybern. 50:363–370, 1984.

[7] Koenderink, van Doorn. *Two-plus-one dimensional differential geometry,* PRL 15(5):439–444, 1994.

[8] Lindeberg. *Scale-space for discrete signals,* PAMI 12(3):234–254, 1990.

[9] Lindeberg. *On scale selection for differential operators,* Proc. 8th SCIA, pp.857–866, 1993.

[10] Lindeberg. *Scale-Space Theory in Computer Vision,* 1994.

[11] Lindeberg. *Edge detection and ridge detection with automatic scale selection,* Proc. CVPR'96, pp.465–470, 1996.

[12] Lindeberg, Gårding. *Shape from texture from a multi-scale perspective,* Proc. 4th ICCV, pp.683–691, 1993.

[13] Wiltschi et al. *Feature Extraction for carbide classification of high speed steel,* Proc. 19th ÖAGM and 1st SDVR, pp.169–176, 1995.

[14] Wiltschi et al. *Image Analysis of Carbide Distributions* Proc. 4th Int. Tooling Conf., pp.213–222, 1996.

[15] Witkin. *Scale-space filtering* Proc. 8th IJCAI, pp.1019–1022, 1983.